Radio Propagation in Open-pit Mines

a First Look at Measurements in the 2.6 GHz Band

Portela Lopes de Almeida, Erika; Caldwell, George; Rodriguez Larrad, Ignacio; Abreu, Sergio; Vieira, Robson; Barbosa, Viviane S. B.; Sørensen, Troels Bundgaard; Mogensen, Preben Elgaard; Uzeda Garcia, Luis Guilherme

Published in:
IEEE 28th Annual International Symposium on Personal, Indoor, and Mobile Radio Communications (PIMRC), 2017

DOI (link to publication from Publisher):
10.1109/PIMRC.2017.8292345

Publication date:
2017

Document Version
Accepted author manuscript, peer reviewed version

Radio Propagation in Open-pit Mines: a First Look at Measurements in the 2.6 GHz Band

Erika P. L. Almeida[1,2], George Caldwell[3], Ignacio Rodriguez[1], Sergio Abreu[2], Robson D. Vieira[3], Viviane S. B. Barbosa[4], Troels B. Sørensen[1], Preben Mogensen[1] and Luis G. Uzeda Garcia[5]

[1]Wireless Communication Networks Section, Department of Electronic Systems, Aalborg University (AAU)
[2]Technology Development Institude (INDT), [3]Ektrum,
[4]Faculdade de Estudos Administrativos de Minas Gerais (FEAD), [5]Instituto Tecnológico Vale (ITV)

***Abstract*—In this paper we present the results of an extensive measurement campaign performed at two large iron ore mining centers in Brazil at the 2.6 GHz band. Although several studies focusing on radio propagation in underground mines have been published, measurement data and careful analyses for open-pit mines are still scarce. Our results aim at filling this gap in the literature. The research is motivated by the ongoing mine automation initiatives, where connectivity becomes critical. This paper presents the first set of results comprising measurements under a gamut of propagation conditions. A second paper detailing sub-GHz propagation is also in preparation. The results indicate that conventional wisdom is wrong, in other words, radio-frequency (RF) propagation in surface mines can be far more elaborate than plain free-space line-of-sight conditions. Additionally, the old mining adage "no two mines alike" seems to remain true in the RF domain.**

I. Introduction

Mining is as old as human civilization, and still remains one of the most essential industrial activities, being responsible for 1% of the workforce worldwide and a revenue of more than 400 billion dollars per year. In traditional operations, radio network planning and optimization are afterthoughts, typically carried out on a reactive basis via trial-and-error procedures. Consequently, coverage holes and data service outages are common. When bespoke Wi-Fi solutions become an insurmountable bottleneck, self-healing IEEE 802.11 mesh networks augmented by proprietary algorithms are the go-to solutions for the vast majority of miners [1]. In short, radio propagation was little more than a nuisance.

However, the decreasing prices of ores, combined with a highly competitive market have been pushing this industry to increase its operational efficiency. In this context, remotely operated, autonomous equipment and systems have emerged as the technical solution promising a broad range of benefits, including enhanced employee health and safety conditions, higher productivity, and reduced environmental impacts. But, given the mobile nature of surface mining equipment, wireless networks have taken center stage as they form the backbone of unmanned operations. As such, proper planning and constant optimization can no longer be overlooked [2], [3].

The quality of radio network planning depends on the accuracy of RF propagation models, and, while channel characterization, propagation measurement results, and models for underground mines have been widely investigated [4], [5], the same cannot be said about open-pit mines, in which only two references were found. In [6], a geometric model is proposed based on the complete knowledge of the environment, so that the direct, reflected and diffracted fields are calculated and used for the prediction of the received field strength at a specific location. In [7] the authors present a study of the channel impulse response in the 2.4 GHz band, based on a set of wideband measurements. Their conclusion is that the increased delay spread, caused by multiple reflections, limits the performance of OFDM systems such as LTE and Wi-Fi with standard cyclic prefix values.

More empirical data is clearly needed, in order to develop and validate large-scale and small-scale channel characterization. While geographic information systems (GIS), ray-tracing techniques and models such as the one proposed in [6] can also play an important role in characterization and optimization of smaller areas, we believe that a simplified model can be helpful for quick determination of link budgets, dominance areas and network capacity in open-pit mines.

Our paper presents a first look at large-scale channel characterization in open-pit mines, considering both macro cell and small cell deployments operating at the 2.6 GHz band. This set of results, collected in distinct scenarios, is used as a starting point for the definition of simple propagation models in this atypical industrial environment.

The remainder of this paper is organized as follows. Section II describes the measurement scenarios and setup. Section III details the data processing and calibration procedures. In Section IV we discuss the measurement results and present empirical path loss models considering the distinct scenarios and base station deployment configurations. Finally, Section IV concludes the paper and outlines future research directions.

II. Measurement Scenario, Setup and Challenges

The selected mines are located in the Iron Quadrangle region in Minas Gerais, Brazil. This region supplies approximately 200 million metric tons of iron ore per year. In order to study the propagation characteristics in open-pit mines, extensive drive-tests were carried out in April and May 2017 (dry weather periods). It is important to mention the many practical

challenges associated with measurement campaigns in such restricted and risky industrial environments: rigorous safety and security protocols, rock blasting procedures that constrain and interrupt the measurement process, unpaved roads and tracks, absolute traffic priority given to haul trucks and large machinery, limited infrastructure for this kind of activity due to the mutant nature of mines, and business pressures. These difficulties might help explain the lack of empirical data in the literature. Considering all these impediments, the criteria used for selecting the transmitter locations were:

- Coverage Planning: with the help of a commercial prediction tool, transmitters were positioned with the aim to cover all relevant areas in the mine (crusher, waste piles, pits).
- Accessibility and safety: regular cars may not access all areas of the mine, especially during the periods when haul trucks are allowed to drive at high speed. Furthermore, the location of transmitters, especially small cells, needs to be safe, blocked and properly signaled. Therefore, this criterion was important in selecting the transmitter locations in different periods of the day.
- Infrastructure availability: we used the existing infrastructure in terms of power sources, towers and cell-on-wheels (COW).
- Coverage holes: prior to the field work, a series of coverage predictions were made in order to determine the ideal location of small cells. The final decision combined this information with suggestions from mine personnel.
- Scenario diversity: whenever possible, small cell locations were chosen to cover distinct scenarios within the mine.

A. Measurement Scenario

Despite all challenges, a vast amount of measurement data was collected: in total, more than 800 km were driven. Figures 1 and 2 illustrate the location of the transmitters in mining complexes 1 and 2, as well as the measurement routes.

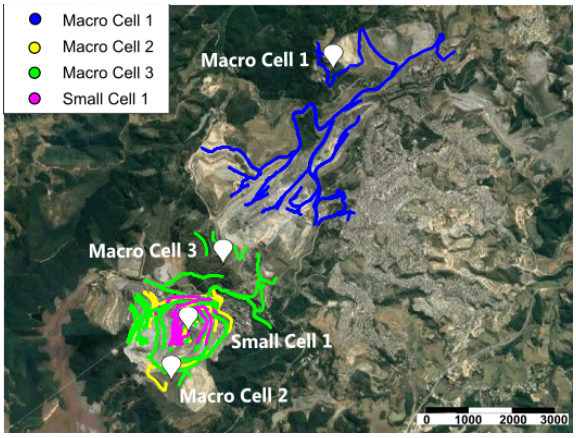

Fig. 1. Measurement routes and transmitter locations at mine 1. The scale is in meters.

The complex in Figure 1 has been mined since 1942 and spans a 12 km long and 5 km wide area. The second mine shown in Figure 2 was inaugurated in 2006 and is at an earlier stage of life. It consists of a single pit and covers an area that is 4 km long and 2.3 km wide.

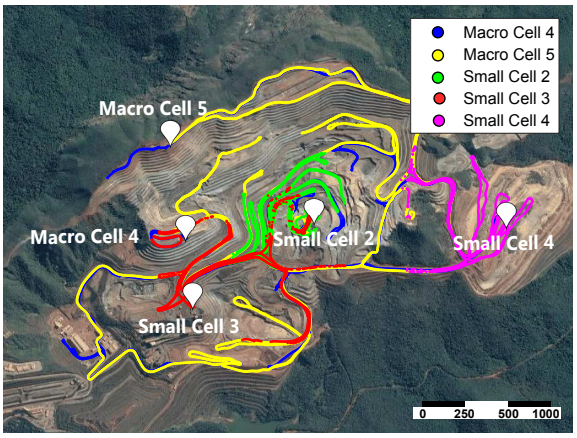

Fig. 2. Measurement routes and transmitter locations at mine 2. The scale is in meters.

Besides the differences in dimensions and lifetime, the mines also differ in terms of terrain profiles. Figures 3 and 4 show, in blue, the altitude of the terrain profile, in meters, as a function of the two-dimensional distance between one of the transmitters and the lowest altitude receiver position for mines 1 and 2, respectively. Mine complex 1 is characterized by the three deep pits, each resembling a hollow inverted pyramid, while mine's 2 pit is actually located on a hillside. For this reason, we will denote mines 1 and 2 as the inverted pyramid mine and the hillside mine, respectively.

B. Measurement Setup

The transmitted signal, a continuous wave (CW), was generated by a Keysight signal generator, and transmitted by an omnidirectional antenna, with 60° elevation beamwidth and 6 dBi gain. Additionally, in macro cell deployments, a power amplifier was used in order to extend the measurement range. The EIRP in each transmitter is described in Table I, as well as the antenna heights in each case.

The receiver was mounted on a vehicle and the omnidirectional antenna, with 3 dBi gain, was placed on the rooftop, at 1.8 m. This vehicle was driven at an average speed of 35 km/h

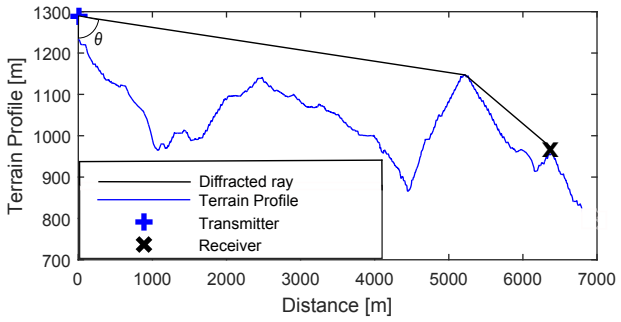

Fig. 3. Altitude of the terrain profile between the transmitter in Macro Cell 1 and the lowest receiver position at the inverted pyramid mine. The figure also shows the diffracted ray and the angle, θ, considered in this NLOS case.

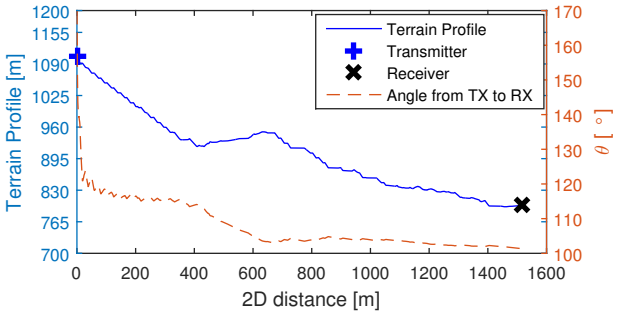

Fig. 4. Altitude of the terrain profile between the transmitter in Macro Cell 5 and the lowest receiver position at the hillside mine. The right y-axis shows the variation of the angle, θ, in this route.

and all the routes were traversed at least twice. The received signal strength and GPS locations were recorded using the R&S TSMW Universal Radio Network Analyzer at a rate of 150 samples/s. In total, more than 8 million raw samples were collected during this measurement campaign.

TABLE I
TRANSMITTERS SETUP

Mine	Transmitter Type	Tx height above ground level [m]	EIRP [dBm]
1	Macro Cell 1	55	47
1	Macro Cell 2	5.5	48
1	Macro Cell 3	42	48
2	Macro Cell 4	40	50
2	Macro Cell 5	5	50.1
1	Small Cell 1	5.5	17.1
2	Small Cell 2	5	17.2
2	Small Cell 3	5	17.2
2	Small Cell 4	3.5	17.3

III. DATA PROCESSING

From the measurements, the the path loss (L) can be estimated by:

$$L_{[dB]} = P_{TX_{[dBm]}} - P_{RX_{[dBm]}} - L_{\text{cables}_{[dB]}} + G_{TX_{[dB]}}(\theta) + G_{RX_{[dB]}} \quad (1)$$

where P_{TX} represents the transmitted power, P_{RX} represents the local mean received power, averaged over distance ranges of 40λ [10], [11], L_{cables} represents the combined cable losses in both Tx and Rx sides, $G_{TX}(\theta)$ and G_{RX} are the Tx and Rx antenna gains, respectively.

Both the Tx and the Rx antennas used in this study are omni-directional in the azimuth plane. Therefore, their gains depend only on the elevation angle, θ, which is calculated based on the transmitter and receiver positions. Figure 4 shows, in red, an example of the elevation angle variation within one of the measurement routes. In that path, the elevation angle varies from 180°, in locations below the transmitter, to 100° in locations far away from it. In order to account for this variation, the gain of the transmitter antenna is compensated accordingly, when there is LOS between transmitter and receiver.

If the LOS is obstructed, the elevation angle depends on the diffracted ray, i.e. it also depends on the position and height of the obstacle relative to the transmitter. This case is illustrated in Figure 3, where we show an example of a diffracted ray and the considered elevation angle. Besides compensating for the transmitter's antenna pattern in LOS and NLOS conditions, we only consider samples collected within the half-power beamwidth (HPBW) of the vertical beam of the transmitter antenna.

On the receiver side, we always assume the maximum antenna gain since the of angle-of-arrival cannot not be easily estimated due to the multiple received paths. Moreover, measurements below the sensitivity level of -115 dBm were filtered out during the post-processing stage.

The analysis proceeds with the parametrization of a statistical large-scale path loss model. We are aware of the existence of different statistical models, such as the alpha-beta (AB) model, the close-in (CI) free-space reference distance model, and the CI model with a frequency-weighted path loss exponent (CIF) [8]. Although the CI and CIF models provide better parameter stability, in this work, we chose the AB model in order to highlight the differences between the considered scenarios (different mines and deployments). The model consists in a linear regression of the L_{dB} estimates considering a floating intercept. The path loss ($PL_{[dB]}$) is modeled as:

$$PL(d)_{[dB]} = \alpha \times 10\log_{10}(d_{[m]}) + \beta \quad (2)$$

The path loss exponent α and the floating intercept β can be obtained by a least squares linear regression of the path loss, L, estimates obtained in Eq. 1:

$$\alpha = \frac{\sum_{n=1}^{N}(D_n - \overline{D})(L_n - \overline{L})}{\sum_{n=1}^{N}(D_n - \overline{D})^2} \quad (3)$$

$$\beta = \overline{L} - \alpha \times \overline{D} \quad (4)$$

where $D_n = 10\log_{10}(d_{n_{[m]}})$ is the 3D distance, in logarithmic scale, between the transmitter and the n^{th} average distance range, and $\overline{D}$ represents the average distance, also in logarithmic scale, over the considered data set. L_n represents the path loss estimate at the n^{th} average point, and $\overline{L}$ represents the average path loss over the considered data set. In order to evaluate how well the model fits with the measurement data, we also consider the root mean square error RMSE:

$$RMSE = \sqrt{\frac{\sum_{n=1}^{N}(L_n - PL_n)^2}{N}} \quad (5)$$

Finally, shadow fading, σ_{SF} is also calculated to account for random variations around the mean path loss:

$$\sigma_{SF} = \sqrt{\frac{\sum(L_n - l_n)^2}{N-1}} \quad (6)$$

where l_n is the mean path loss over segments of 50 meters.

IV. Results and Discussion

The results are shown for macro and small cells separately. However, although the deployment of macro and small cells is a reality in open-pit mines [1], there is no clear definition of what a small cell and a macro cell are in this scenario. Macro and small cell scenarios are normally defined considering heterogeneous networks deployed in urban environments. In that case, from a radio propagation perspective, macro cells are defined as those deployed in elevated outdoor position, above the rooftop of the building, typically, with transmit power higher than 24 dBm. Small cells, on the other hand, are defined as those deployed below rooftop of the building in outdoor or indoor positions, with lower transmit power [12]. The use of the same definition is clearly not possible in this scenario.

Therefore, we propose the following definition, based on the transmitter location relative to the terrain profile: a small cell deployment is defined as the one where the transmitter is placed close to the ground level, below the median altitude of the covered area. The macro cell deployment, on the other hand, is defined as the one where the transmitter is placed in elevated positions, above the median altitude of the coverage area.

The definition becomes clearer in Figure 5, in which the cumulative distributions of the altitude difference between the receiver and the transmitter, for each one of the transmitters, are presented. Positive altitudes are those in which the receiver is above the transmitter, and negative altitudes occur when the receiver is below the transmitter. In general, all small cells, but small cell number 3, have at least 60% of the measured locations above the transmitter height. Concerning the macro cells, all of them, but macro cell number 4, are located above the receiver, considering all the measurement routes. Small cell 3 is "on the border" of our definition of macro and small cells.

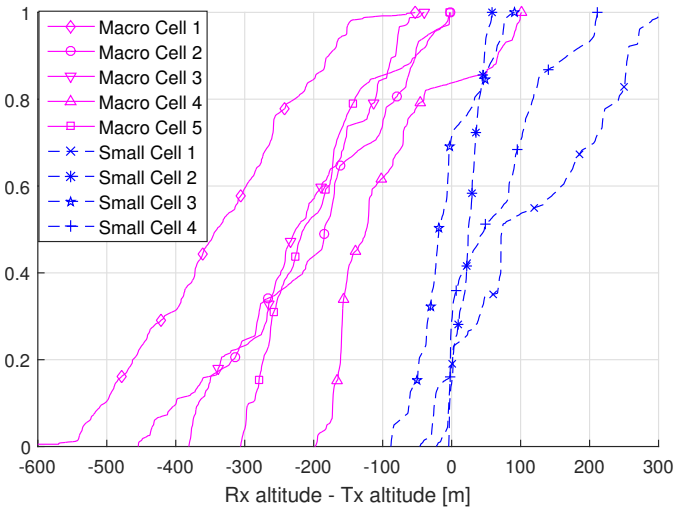

Fig. 5. CDF plot of the difference between the receiver altitude and the transmitter altitude for all transmitters.

Using the model presented in Section III, we define path loss models for the transmitters. At first, a simple linear regression, using all the points measured for a given transmitter, is done. The path loss exponents, α, are shown in Table II for all macro and small cell transmitters measured in the mines. This Table also shows the percentage of LOS and NLOS locations within each coverage area. Through a simple path loss exponent classification, three groups were observed.

TABLE II
Path loss exponent and LOS and NLOS percentage

Transmitter	**LOS [%]**	**NLOS [%]**	α
Macro Cell 1	43	57	2.1
Macro Cell 2	62	38	1.5
Macro Cell 3	78	22	2.1
Macro Cell 4	78	22	2.9
Macro Cell 5	65	35	2.7
Small Cell 1	22	78	3.3
Small Cell 2	19	81	3.6
Small Cell 3	54	45	3.6
Small Cell 4	39	61	3

The first group contains the macro cells deployed in the inverted pyramid mine, mine 1, described in Section II, which encompasses at least 3 large and deep pits, where most of the measurements were concentrated. The propagation in this group is characterized by path loss exponents between 1.5 and 2.1. Path loss exponents below the free space path loss (FSPL) exponent have been found previously in the vast literature on radio propagation in underground mines, due to the waveguide effect caused by multiple reflections on tunnel walls, floor and ceiling [5], [13]. Although the experiment presented here does not permit us to conclude that the same effect is present in the mine, we believe that this phenomenon should be further investigated also in the open-pit mine scenario.

The second group contains the macro cells deployed in mine 2, the hillside mine. This mine, as previously mentioned, is in much earlier iron ore exploration, therefore the pit is not so deep as in mine 1. Although both scenarios consist of macro cells, the path loss exponents in mine 2, the inverted pyramid mine, are higher than those observed the hillside mine, mine 1: between 2.7 and 2.9. This is an indication that a simple path loss model cannot be generalized for macro cell deployments in open-pit mines.

Finally, group 3 is composed of all small cells of both mines, and the path loss exponents are between 3 and 3.6. The larger exponent is expected considering that these transmitters are located below the median terrain altitude, placed just a few meters above the ground level when compared to the macro cells. Besides NLOS conditions caused by obstacles in the propagation path, small cells are also subject to NLOS caused by the geometry (in terms of distances and antenna heights) of transmitter and receiver: obstructions of the propagation path also occur when the first Fresnel zone touches the ground. In small cells, this location is closer to the transmitter than

in macro cells, because they are placed closer to the ground level. However, due to terrain irregularities, the determination of the exact breakpoint distance is trickier in mine scenarios.

The LOS/NLOS percentage, also in Table II, was investigated with the aid of digital terrain maps (DTM), with a 1 m resolution. In general, as in other scenarios, macro cells have a higher percentage of LOS samples, and small cells deployments present a higher percentage of NLOS samples. The exceptions are Macro cell 1 and Small cell 3. Macro cell 1 coverage area is mostly obstructed by at least one hill, as in Figure 3, which explains the higher percentage of NLOS locations. Small cell 3, on the other hand, is at the border of our definition of macro and small cells, and part of the measured points are below the transmitter altitude. LOS and NLOS percentages are strongly dependent on specific terrain characteristics.

Based on the previous observations - path loss exponents and percentages of LOS/NLOS samples - we propose single slope models for macro cell deployments, one for each mine, and a dual slope model for small cell deployments in open-pit mines.

The macro cell path loss estimates and models are presented in Figures 6 and 7 for each mine. LOS samples are plotted in blue, and NLOS samples are plotted in red. In black, the dashed line represents the single slope model, and the solid line represents the FSPL model, for comparison.

From the results, it is observed that in macro cells deployments, LOS and NLOS locations are mixed all along the distance between transmitter and receiver locations. This indicates that NLOS condition is caused by terrain obstructions, that affect specific measurement routes, rather than only by the transmitters and receivers geometries, in terms of antenna heights and distances. From the path loss results in those figures, it is also possible to notice the higher variability of the terrain in the inverted pyramid mine, mine 1, when compared to the hillside mine, mine 2. In Figure 6, the two arrows show how the obstacles in the terrain impact on the fluctuations over the path loss model. The terrain variability in this mine also explains the difference of 20 dB considering the FSPL model.

The results are further detailed in Tables III and IV. The last line of each table shows the aggregated models, fitted over all the collected data of transmitters in groups 1 and 2, respectively. The model is defined in terms of path loss exponent, α, intercept, β, shadowing σ_{SF} and RMSE. The results show a clear difference in propagation mechanisms between macro cell deployments in the inverted pyramid mine, mine 1, and in the hillside mine, mine 2, as discussed previously in Table II. The inverted pyramid mine aggregated results show an exponent of 2.1, in comparison to 2.8 measured in the hillside mine.

On small cell deployments, although there are distances with mixed LOS and NLOS samples, there is a clear transition distance between them where the propagation is mainly characterized by NLOS points. These cells are closer to the ground level, and the breakpoint distance, where the path loss exponent changes, occurs closer to the transmitter.

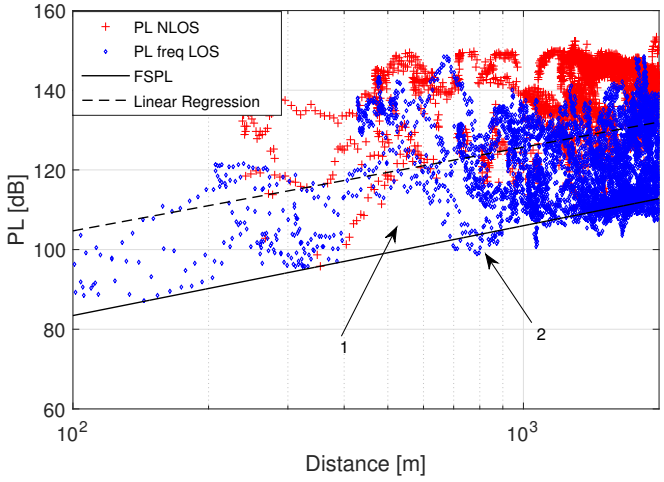

Fig. 6. Combined path loss and linear regression considering aggregated LOS and NLOS samples for all Macro Cell transmitters in the inverted pyramid mine (1).

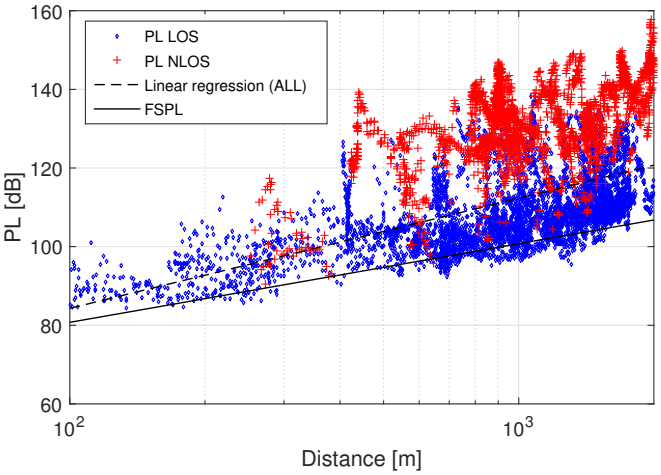

Fig. 7. Path loss and linear regressions considering LOS and NLOS samples, for all Macro Cell transmitters in the hillside mine (2).

TABLE III
SUMMARY OF THE PARAMETERS OF THE PROPOSED MACRO CELL PATH LOSS MODEL, INVERTED PYRAMID MINE (1)

	α	β	σ_{SF}	RMSE
Macro Cell 1	2.1	59.9	11.1	12.4
Macro Cell 2	1.5	74.7	8.8	12.7
Macro Cell 3	2.1	64	9.1	10.5
All Cells	**2.1**	**62.7**	**12.3**	**12**

For this reason, the results are presented as a function of the obstruction, or not, of the LOS. Figure 8 shows the path loss estimates and models considering the aggregated samples of all transmitters in group 3 and Table V summarizes the models for each one of the transmitters in the group, as well as the

TABLE IV
SUMMARY OF THE PARAMETERS OF THE PROPOSED MACRO CELL PATH LOSS MODEL, HILLSIDE MINE (2).

	α	β	σ_{SF}	RMSE
Macro Cell 4	2.9	25.6	10.6	12
Macro Cell 5	2.7	33.9	9.9	12.5
All Cells	**2.8**	**29.8**	**11**	**12.4**

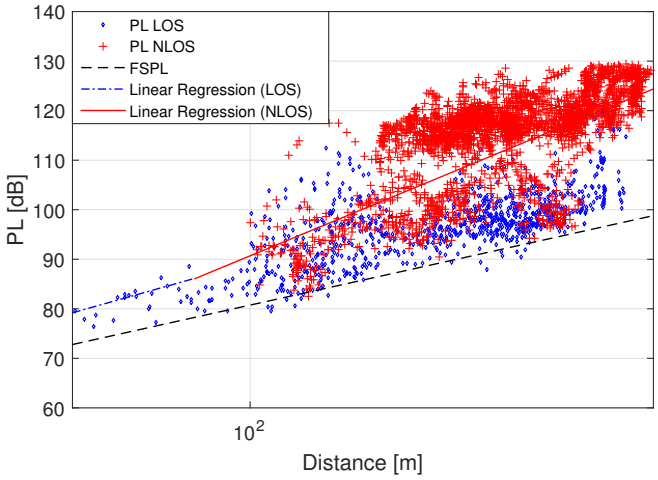

Fig. 8. Path loss and linear regressions considering LOS and NLOS samples, for all Small Cell transmitters in mines 1 and 2.

combined model. The results of the NLOS conditions of small cell 3 are omitted due to a limitation in our measurement setup: there was not enough measurement range to fit a model. The path loss exponent is 2.5 in LOS, and 3.7 in NLOS. Since we proposed a distinct model for LOS and NLOS, the RMSE, and shadowing values are reduced when compared to the macro cell cases.

V. CONCLUSION

To the best of our knowledge, this paper presents the first empirical study of the large-scale radio propagation in iron ore open-pit mines at the 2.6 GHz frequency band. An extensive measurement campaign was carried out in two large mining complexes located in the southeast of Brazil, where 9 transmitters were deployed in macro- and small-cell scenarios. Considering the topographic contrast between an open-pit environment and rural or urban scenarios, we rediscussed the notion of macro and small cells.We have also presented preliminary path loss models for both types of deployments.The results show that the geometry of the mines impacts the path loss exponent, implying that there are no two mines alike.

This work is part of ongoing research effort which will gradually cover other propagation characteristics in open-pit mines, such as shadowing, small-scale phenomena, and the extension to other frequency bands of interest. Our final objective is to characterize the mobile radio propagation channel in iron open-pit mines in order to support the operation of autonomous and teleoperated equipment in this challenging environment. In a broader sense, the results are of interest to those working on next radio technology and its industrial applications.

TABLE V
SUMMARY OF THE PARAMETERS OF THE PROPOSED SMALL CELL PATH LOSS MODEL

		α	β	σ_{SF}	RMSE
Small Cell 1	LOS	2.5	40.5	6.3	7.3
	NLOS	3.9	10.8	7.3	7.6
Small Cell 2	LOS	2.1	48.9	5	5.8
	NLOS	3	41	5.3	4.9
Small Cell 3	LOS	2.9	32	5.3	5.9
	NLOS	-	-	-	-
Small Cell 4	LOS	2.4	39.1	5.5	5.7
	NLOS	3.5	15.9	5.5	7.8
All Cells	**LOS**	**2.5**	**38.5**	**7.5**	**6**
	NLOS	**3.7**	**15.9**	**7.2**	**7.9**

ACKNOWLEDGMENT

The authors would like to thank the automation, telecommunications, mineral exploration cartography, and IT teams from Vale S.A. for their valuable inputs and help.

REFERENCES

[1] Vellingiri, S., Tandur, D., Kande, M. *Energy efficient wireless infrastructure solution for open pit mine.* Advances in Computing, Communications and Informatics (ICACCI)(2013): 1463-1467.

[2] Garcia, Luis G. Uzeda, et al. *Mission-critical mobile broadband communications in open-pit mines.* IEEE Communications Magazine 54.4 (2016): 62-69.

[3] Barbosa, Viviane SB, et al. *The Challenge of Wireless Connectivity to Support Intelligent Mines.* 24th World Mining Conference (wmc) 2016.

[4] Sun, Zhi, and Ian F. Akyildiz. Channel modeling and analysis for wireless networks in underground mines and road tunnels. *Communications, IEEE Transactions on 58.6 (2010)*: 1758-1768.

[5] Forooshani, Arghavan Emami, et al. A survey of wireless communications and propagation modeling in underground mines. *Communications Surveys & Tutorials, IEEE 15.4 (2013):* 1524-1545.

[6] J J Aitken, Development of a radio propagation model for an open cut mine, *20th International Electronics convention & exhibition*, 1985.

[7] Nilsson, Rickard, and Jaap van de Beek. Channel Measurements in an Open-pit Mine using USRPs: 5G–Expect the Unexpected. *Wireless Communications and Networking Conference (WCNC)*, 2016.

[8] Sun, Shu, et al. *Investigation of prediction accuracy, sensitivity, and parameter stability of large-scale propagation path loss models for 5G wireless communications.* IEEE Transactions on Vehicular Technology 65.5 (2016): 2843-2860.

[9] J. D. Parsons. *The Mobile Radio Propagation Channel, 2nd Edition*. Wiley Europe, November 2000.

[10] W. C. Y. Lee, *Mobile Communications Engineering*, 2nd Edition, McGraw Hill, 1983.

[11] Adawi, Nadia S., et al. *Coverage Prediction for mobile radio systems operating in the 800/900 MHz frequency-range*. IEEE Vehicular technology society comittee on radio propagation. IEEE Transactions on vehicular technology 37.1 (1988).

[12] Rodriguez, Ignacio. *An Empirical Study on Radio Propagation in Heterogeneous Networks: with Focus on Mobile Broadband Networks and Small Cell Deployment*. Diss. Aalborg Universitetsforlag, 2016.

[13] Liénard, Martine, and Pierre Degauque. *Natural wave propagation in mine environments.* IEEE Transactions on Antennas and Propagation 48.9 (2000): 1326-1339.